Structure of the Λ(1405) from Hamiltonian effective field theory

Zhan-Wei Liu,[1] Jonathan M. M. Hall,[1] Derek B. Leinweber,[1] Anthony W. Thomas,[1,2] and Jia-Jun Wu[1]

[1]*Centre for the Subatomic Structure of Matter (CSSM), Department of Physics,*
University of Adelaide, Adelaide SA 5005, Australia
[2]*ARC Centre of Excellence for Particle Physics at the Terascale, Department of Physics,*
University of Adelaide, Adelaide SA 5005, Australia

The pole structure of the Λ(1405) is examined by fitting the couplings of an underlying Hamiltonian effective field theory to cross sections of K^-p scattering in the infinite-volume limit. Finite-volume spectra are then obtained from the theory, and compared to lattice QCD results for the mass of the Λ(1405). Momentum-dependent, nonseparable potentials motivated by the well-known Weinberg-Tomozawa terms are used, with SU(3) flavor symmetry broken in the couplings and masses. In addition, we examine the effect on the behavior of the spectra from the inclusion of a bare triquarklike isospin-zero basis state. It is found that the cross sections are consistent with the experimental data with two complex poles for the Λ(1405), regardless of whether a bare-baryon basis state is introduced or not. However, it is apparent that the bare baryon is important for describing the results of lattice QCD at high pion masses.

I. INTRODUCTION

Strange quark phenomenology has always been of great interest to both theoretical and experimental physicists. It exhibits some properties of both light and heavy quarks. However, unlike either the light quark limit or the heavy quark limit, it is difficult to explain the phenomena of strange quark physics comprehensively simply by applying chiral symmetry for zero-mass quarks and heavy-quark symmetry for infinite-mass quarks. Corrections to these symmetries and the treatment of symmetry-breaking effects provide important insight into the internal structure of hadrons.

A. The Λ(1405)

The Λ(1405) is a resonant state with strangeness number $S = -1$, and $I(J^P) = 0(\frac{1}{2}^-)$. It also has been shown to interact strongly with nearby meson-baryon states, the details of which are intimately dependent on its internal structure. The Λ(1405) is close to the threshold of $\bar{K}N$ and mainly decays to the $\pi\Sigma$ state. With the interactions of just these two channels in a Hamiltonian model, the data of $\bar{K}N$ scattering at low energy can be fit well, and the Λ(1405) resonance can be generated. Corrections from the interaction with $\eta\Lambda$ and $K\Xi$ are also usually considered in studying this problem.

A two-pole structure of the Λ(1405) has been proposed in many works [1–4]. Many groups claim these two poles lie on one Riemann sheet. Besides the traditional pole around $1420 - 25i$ MeV, there is another pole with the position varying widely in different models or in different fits [5–7]. The second pole is not mentioned in every work [8].

B. Three-quark core contributions

The basis of the quark model is that there is a three-quark state which provides the dominant contribution to the properties of all baryons. For example, the nucleon is considered to be dominated by a bare nucleon state dressed by smaller contributions from πN, $\pi\Delta$, etc. [9,10]. However, the discussion regarding the Λ(1405) remains ongoing, and deserves careful analysis.

Lattice QCD calculations are able to excite the Λ(1405) with local three-quark operators [11–13] suggesting a nontrivial role for a three-quark component. However, lattice QCD calculations of the strange magnetic form factor of the Λ(1405) have revealed the Λ(1405) to be dominated by a molecular $\bar{K}N$ bound state at light quark masses [13,14]. Attraction between the $\bar{K}$ and N provides clustering which avoids the common volume suppression of weak-scattering states. A small bare-state component also provides a mechanism for the excitation of this state with local three-quark operators.

As one varies the light quark mass in lattice QCD, one expects that the "bare," triquark state will tend to be more important as chiral loops are suppressed in that region [13–15]. For example, one can fit the experimental data very well in the absence of a bare-state contribution with the aforementioned two-particle channels [16]. Such an approach also gives good predictions for the lattice results at small pion masses where the unitary chiral extrapolation works.

However, in the high-pion-mass region the energies of the lattice QCD eigenstates in the finite volume spectrum are much smaller than the thresholds of the reaction channels. It is not possible to form a bound state with a binding energy of more than 100 MeV without a large

increase in the coupling parameters as the pion mass increases. While this cannot be ruled out by our analysis, we consider the interpretation in terms of a bare (three-quark) state to be more natural.

Identification of the $\Lambda(1405)$ in the finite volume of the lattice was performed [13,14] using a simple Hamiltonian effective field theory model focusing on the flavor singlet couplings of the $\pi\Sigma$, $\bar{K}N$, $\eta\Lambda$, and $K\Xi$ channels to the bare basis state required by the admission of a three-quark configuration carrying the quantum numbers of the $\Lambda(1405)$. Having established that the $\Lambda(1405)$ is a molecular $\bar{K}N$ bound state [13,14] it is important to examine the finite-volume spectrum in a calculation that does not distinguish the flavor symmetry of the isospin-zero state. One should not only examine the $\Lambda(1405)$, but also examine the low-lying excitations observed in Ref. [11], associated with the octet-flavor interpolating fields used in the lattice correlation matrix.

C. Models of the $\Lambda(1405)$

Many models have been applied to the $\Lambda(1405)$ [1–8,13,14,16–29]. Beginning with the study based on SU(3) chiral symmetry within the cloudy bag model [27,28], Weinberg-Tomozawa terms have been successful in describing the most prominent interactions. Dimensional regularization was used in solving the Bethe-Salpeter equation with the full Weinberg-Tomozawa potential in Refs. [7,21]. It is also common to use a K-matrix approach in which the potentials are used with an on-shell approximation to obtain the scattering amplitude [2,5,20]. In that case, the potential is often taken to be momentum independent. Regularization with a cutoff was taken in Refs. [8,25]. Separable potentials are favored since they are easy to solve [8].

Rather than effective Weinberg-Tomozawa potential, hadron-exchange potentials are used to study $\Lambda(1405)$ [30,31]. This dynamical coupled-channel approach is also discretized to study the spectrum on the lattice [32].

In this work, we use Hamiltonian effective field theory to analyze both the available experimental data in infinite volume and the results from lattice QCD at finite volume. Hamiltonian effective field theory is a powerful tool for analyzing the lattice results and examining the structure of the states on the lattice [13,14,33–36]. Moreover, it can be applied to calculate the scattering processes in infinite volume. The Weinberg-Tomozawa potentials are included in a Hamiltonian model of the $\Lambda(1405)$, which matches finite-volume effective field theory. The on-shell approximation is not used, and thus the potentials are momentum dependent and nonseparable. The effect of the bare baryon is carefully examined by comparing the results of two scenarios, with and without a bare baryon basis state in the formulation of the Hamiltonian matrix. The two-pole structure of the $\Lambda(1405)$ is also examined.

D. Outline

The formalism for our Hamiltonian effective field theory is presented in Sec. II. In constructing the Hamiltonian, we consider two scenarios: one in which the $\Lambda(1405)$ is dynamically generated purely from the $\pi\Sigma$, $\bar{K}N$, $\eta\Lambda$, and $K\Xi$ interactions, and one also including a bare-baryon basis state to accommodate a three-quark configuration carrying the quantum numbers of the $\Lambda(1405)$.

The forms of the interactions are described in Sec. II A. We then proceed to solve the Bethe-Salpeter equation and obtain the cross sections and pole positions at infinite volume via the T-matrix in Sec. II B. To compare with lattice QCD results, the Hamiltonian is discretized in Sec. II C and solved to obtain results at finite volume.

In Sec. III, the numerical results are presented. The experimental data for $\bar{K}N$ scattering is fit in Sec. III A and the calculation is extended to varying quark masses in Sec. III B. Then the finite-volume spectrum of the Hamiltonian model in our two scenarios is compared to lattice QCD results. Section III C presents results in the absence of a bare-baryon basis state and Sec. III D illustrates how the inclusion of a bare-baryon basis state resolves discrepancies and provides an explanation of which states are seen in contemporary lattice QCD calculations. A brief summary concludes in Sec. IV.

II. FRAMEWORK

A. Hamiltonian

To study the data relevant to the $\Lambda(1405)$, we consider the interactions among $|\pi\Sigma\rangle$, $|\bar{K}N\rangle$, $|\eta\Lambda\rangle$, $|K\Xi\rangle$, and the isospin-1 channel $|\pi\Lambda\rangle$. We use the following Hamiltonian to describe the interactions:

$$H^I = H_0^I + H_{\mathrm{int}}^I, \tag{1}$$

where the superscript I is the isospin.

In the center-of-mass frame, the kinetic-energy Hamiltonian H_0^I is written as

$$H_0^I = \sum_{B_0} |B_0\rangle m_B^0 \langle B_0| + \sum_\alpha \int d^3\vec{k}$$
$$\times |\alpha(\vec{k})\rangle [\omega_{\alpha_M}(k) + \omega_{\alpha_B}(k)] \langle \alpha(\vec{k})|, \tag{2}$$

where $|\alpha\rangle = |\pi\Sigma\rangle, |\bar{K}N\rangle, \ldots$ and

$$\omega_X(k) = \sqrt{m_X^2 + k^2} \tag{3}$$

is the noninteracting energy of particle X. The subscripts α_M and α_B represent the meson and baryon separately in channel α.

The interaction Hamiltonian of this system includes two parts

$$H_{\text{int}}^I = g^I + v^I. \tag{4}$$

g^I describes the vertex interaction between the bare-baryon and two-particle channels α

$$g^I = \sum_{\alpha, B_0} \int d^3\vec{k} \{ |\alpha(\vec{k})\rangle G_{\alpha, B_0}^{I\dagger}(k) \langle B_0 |$$
$$+ |B_0\rangle G_{\alpha, B_0}^I(k) \langle \alpha(\vec{k})| \}, \tag{5}$$

where we use the form of the ordinary S-wave coupling for G^I

$$G_{\alpha, B_0}^I(k) = \frac{\sqrt{3} g_{\alpha, B_0}^I}{2\pi f} \sqrt{\omega_\pi(k)} u(k). \tag{6}$$

A dipole form factor, $u(k) = (1 + k^2/\Lambda^2)^{-2}$, with regulator parameter $\Lambda = 1$ GeV is used to regulate the calculation. In the scenario without a bare baryon, we set the couplings $g_{\alpha, B_0}^I = 0$ to turn off the effect of $|B_0\rangle$.

The use of a dipole regulator has received a great deal of attention in the literature. It has been clearly established that this approach, known as finite-range regularization (FRR), is equivalent to dimensionally regulated chiral perturbation theory (χPT) in the power counting regime [37,38], roughly below a 300-MeV pion mass, corresponding to the few lowest lattice data points. At higher pion masses the formal χPT expansion fails to converge. FRR provides a model for the behavior of the chiral loops at larger meson mass which has proven successful over a very wide range of pion masses for many observables. By fitting the theory to both the experimental data and the lattice data, the other parameters in the model acquire an implicit dependence on the regulator parameter, which removes the formal dependence on that mass parameter. In our work, all parameters and the bare-state mass are appropriate to the regulator mass used, namely, 1 GeV.

We define the direct two-to-two particle interaction v^I by

$$v^I = \sum_{\alpha, \beta} \int d^3\vec{k} d^3\vec{k'} |\alpha(\vec{k})\rangle V_{\alpha, \beta}^I(k, k') \langle \beta(\vec{k'})|, \tag{7}$$

where we use the potential derived from the Weinberg-Tomozawa term [39]

$$V_{\alpha, \beta}^I(k, k') = g_{\alpha, \beta} \frac{[\omega_{\alpha_M}(k) + \omega_{\beta_M}(k')] u(k) u(k')}{8\pi^2 f^2 \sqrt{2\omega_{\alpha_M}(k)} \sqrt{2\omega_{\beta_M}(k')}}. \tag{8}$$

We do not use the so-called on-shell approximation in this work. We keep the form $\omega_{\alpha_M}(k) + \omega_{\beta_M}(k')$ rather than replacing it with $2E - m_{\alpha_B} + m_{\beta_B}$ in Eq. (8). Our potentials are momentum dependent and not separable.

B. *T*-Matrix

We can evaluate the T-matrices for two-particle scattering by solving a three-dimensional reduction of the coupled-channel Bethe-Salpeter equation in each partial wave

$$T_{\alpha, \beta}^I(k, k'; E)$$
$$= \tilde{V}_{\alpha, \beta}^I(k, k'; E) + \sum_\gamma \int q^2 dq$$
$$\times \tilde{V}_{\alpha, \gamma}^I(k, q; E) \frac{1}{E - \omega_\gamma(q) + i\epsilon} T_{\gamma, \beta}^I(q, k'; E), \tag{9}$$

where $\omega_\alpha(k)$ is the total kinetic energy of channel α,

$$\omega_\alpha(k) = \sqrt{m_{\alpha_1}^2 + k^2} + \sqrt{m_{\alpha_2}^2 + k^2}, \tag{10}$$

and the coupled-channel potential can be obtained from the interaction Hamiltonian

$$\tilde{V}_{\alpha, \beta}^I(k, k'; E) = \sum_{B_0} G_{\alpha, B_0}^{I\dagger}(k) \frac{1}{E - m_B^0} G_{\beta, B_0}^I(k')$$
$$+ V_{\alpha, \beta}^I(k, k'). \tag{11}$$

The cross section $\sigma_{\tilde{\alpha}, \tilde{\beta}}$ for the process $\bar{\beta} \to \bar{\alpha}$ is

$$\sigma_{\tilde{\alpha}, \tilde{\beta}} = \frac{4\pi^3 k_{\text{cm}}^\alpha \omega_{\alpha_M}^{\text{cm}} \omega_{\alpha_B}^{\text{cm}} \omega_{\beta_M}^{\text{cm}} \omega_{\beta_M}^{\text{cm}}}{E_{\text{cm}}^2 k_{\text{cm}}^\beta} |T_{\tilde{\alpha}, \tilde{\beta}}(k_{\text{cm}}^\alpha, k_{\text{cm}}^\beta; E_{\text{cm}})|^2, \tag{12}$$

where $T_{\tilde{\alpha}, \tilde{\beta}}$ is the linear combination of $T_{\alpha, \beta}^0$ and $T_{\alpha, \beta}^1$ multiplied by the corresponding Clebsch-Gordan coefficients, e.g., $T_{\bar{K}^0 n, K^- p} = -1/2 T_{\bar{K}N, \bar{K}N}^0 + 1/2 T_{\bar{K}N, \bar{K}N}^1$. The superscript and subscript "cm" refer to the center-of-mass frame.

To find the poles of $T_{\alpha, \beta}^0(k, k'; E_{\text{pole}})$, we replace the integration variable q with $q \times \exp(-i\theta)$, for $\gamma = \pi\Sigma$ in Eq. (9), and maintain $0 \ll \theta < \pi/2$. That is, we search for poles of the $\Lambda(1405)$ on the second Riemann sheet, which is adjacent to the physical sheet separated by the cut between the $\pi\Sigma$ and $\bar{K}N$ thresholds.

C. Finite-volume matrix Hamiltonian model

We can discretize the Hamiltonian in a box with length L for $I = 0$. A particle can only carry momenta $k_n = \sqrt{n} 2\pi/L$ in the box, where $n = 0, 1, \ldots$. The noninteracting isospin-zero Hamiltonian can be written as

$$\mathcal{H}_0^0 = \text{diag}\{m_B^0, \omega_{\pi\Sigma}(k_0), \omega_{\bar{K}N}(k_0), \ldots, \omega_{\pi\Sigma}(k_1), \ldots\}, \tag{13}$$

and the interacting Hamiltonian is

$$\mathcal{H}_{\text{int}}^0 = \begin{pmatrix} 0 & \mathcal{G}_{\pi\Sigma,B_0}^0(k_0) & \mathcal{G}_{\bar{K}N,B_0}^0(k_0) & \cdots & \mathcal{G}_{\pi\Sigma,B_0}^0(k_1) & \cdots \\ \mathcal{G}_{\pi\Sigma,B_0}^0(k_0) & \mathcal{V}_{\pi\Sigma,\pi\Sigma}^0(k_0,k_0) & \mathcal{V}_{\pi\Sigma,\bar{K}N}^0(k_0,k_0) & \cdots & \mathcal{V}_{\pi\Sigma,\pi\Sigma}^0(k_0,k_1) & \cdots \\ \mathcal{G}_{\bar{K}N,B_0}^0(k_0) & \mathcal{V}_{\bar{K}N,\pi\Sigma}^0(k_0,k_0) & \mathcal{V}_{\bar{K}N,\bar{K}N}^0(k_0,k_0) & \cdots & \mathcal{V}_{\bar{K}N,\pi\Sigma}^0(k_0,k_1) & \cdots \\ \vdots & \vdots & \vdots & \ddots & \vdots & \ddots \\ \mathcal{G}_{\pi\Sigma,B_0}^0(k_1) & \mathcal{V}_{\pi\Sigma,\pi\Sigma}^0(k_1,k_0) & \mathcal{V}_{\pi\Sigma,\bar{K}N}^0(k_1,k_0) & \cdots & \mathcal{V}_{\pi\Sigma,\pi\Sigma}^0(k_1,k_1) & \cdots \\ \vdots & \vdots & \vdots & \ddots & \vdots & \ddots \end{pmatrix}, \quad (14)$$

where

$$\mathcal{G}_{\alpha,B_0}^0(k_n) = \sqrt{\frac{C_3(n)}{4\pi}}\left(\frac{2\pi}{L}\right)^{3/2} G_{\alpha,B_0}^0(k_n), \quad (15)$$

$$\mathcal{V}_{\alpha,\beta}^0(k_n,k_m) = \frac{\sqrt{C_3(n)C_3(m)}}{4\pi}\left(\frac{2\pi}{L}\right)^3 V_{\alpha,\beta}^0(k_n,k_m). \quad (16)$$

$C_3(n)$ represents the number of ways of summing the squares of three integers to equal n.

One obtains the energy levels and the composition of the energy eigenstates in finite volume by solving the eigen-equation of the total isospin-zero Hamiltonian $\mathcal{H}^0 = H_0^0 + \mathcal{H}_{\text{int}}^0$. The results can be confronted with results from lattice QCD to evaluate the merit of the model.

III. NUMERICAL RESULTS AND DISCUSSION

In this section, the cross sections of K^-p and the eigenenergy spectrum for the $\Lambda(1405)$ are calculated in our two scenarios: one in which the $\Lambda(1405)$ is dynami-cally generated purely from the $\pi\Sigma$, $\bar{K}N$, $\eta\Lambda$, and $K\Xi$ interactions, and one also including a bare-baryon basis state to accommodate a three-quark configuration carrying the quantum numbers of the $\Lambda(1405)$. The poles for the $\Lambda(1405)$ resonance are determined, and the associated structure is examined.

First, we obtain the couplings of the Hamiltonian field theory by fitting the cross sections of $K^-p \to K^-p$, $K^-p \to \bar{K}^0 n$, $K^-p \to \pi^-\Sigma^+$, $K^-p \to \pi^0\Sigma^0$, and $K^-p \to \pi^+\Sigma^-$, and $K^-p \to \pi^0\Lambda$ at infinite volume. With these couplings, the eigenenergy levels can be calculated at finite volume. We compare them with the lattice QCD results and discuss the structure of the $\Lambda(1405)$.

A. Cross sections and poles

Interactions in both the $I = 0$ and $I = 1$ channels contribute to the cross sections of K^-p. Since the aim of this work is to study the $\Lambda(1405)$ at $I = 0$, we include $\pi\Sigma$, $\bar{K}N$, $\eta\Lambda$, and $K\Xi$ channels for $I = 0$, while we only include $\pi\Sigma$, $\bar{K}N$, and $\pi\Lambda$ channels for $I = 1$.

Since the threshold of $\eta\Lambda$ and $K\Xi$ are far away from the energy region of experimental data, the cross sections are not very sensitive to their couplings. Therefore, we set $g_{\bar{K}N,\eta\Lambda}^0$, $g_{\pi\Sigma,K\Xi}^0$, $g_{\eta\Lambda,K\Xi}^0$, and $g_{K\Xi,K\Xi}^0$ at their $\text{SU}_f(3)$-limit couplings but with one global adjustable constant g_0,

$$g_{\bar{K}N,\eta\Lambda}^0 = -3/\sqrt{2}g_0, \qquad g_{\pi\Sigma,K\Xi}^0 = -\sqrt{3/2}g_0,$$
$$g_{\eta\Lambda,K\Xi}^0 = 3/\sqrt{2}g_0, \qquad g_{K\Xi,K\Xi}^0 = -3g_0. \quad (17)$$

Comparing our two scenarios, the difference lies mainly in the $I = 0$ channel where a bare baryon can be included or omitted. We first fit the cross sections in the scenario without a bare baryon. After that, we leave the couplings in the channel $I = 1$ fixed, and adjust those in the $I = 0$ channel when incorporating a bare-baryon contribution.

Just with limited experimental data for cross sections, we obtained a bare mass which can generate a pole close to that of $\Lambda(1670)$. The mass is far away from the fit energy region, and the properties of the bare state suffer from large uncertainties. In addition to the data for cross sections, we also fit the two masses from the CSSM group at the largest two pion masses and make the pole in the infinite volume close to $(1670 \pm 10) - (18 \pm 7)i$ MeV at the same time in the second scenario.

The results of our fits to the cross sections with Eq. (12) are illustrated in Fig. 1. The cross sections are described well, regardless of whether a bare-baryon contribution is introduced in the $I = 0$ channel or not. The fit parameters are provided in Table I.

Two poles are found for the $\Lambda(1405)$ in both scenarios. The pole positions are consistent with results from other groups, briefly reviewed in Table II. The real parts of the poles are very close to the thresholds of $\bar{K}N$ and $\pi\Sigma$.

In our scenario without the bare state, we cannot find a pole for $\Lambda(1670)$. However, in the scenario with the bare baryon, we can find a pole corresponding to $\Lambda(1670)$ at $1660 - 30i$ MeV. Our result provides a possible candidate for Lambda(1670) which is mainly a bare state in our model.

The small differences in the K^-p cross sections and the $\Lambda(1405)$ pole positions between the two scenarios indicate
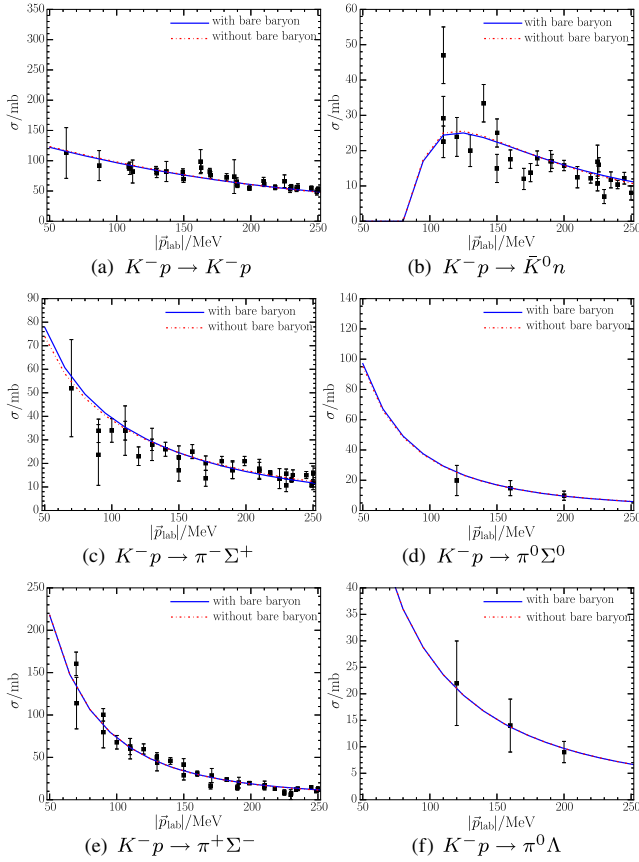
FIG. 1. Experimental data and our fits to the cross sections of $K^- p$. The solid lines are for our scenario with a bare-baryon component included in the $I = 0$ channel, and the dashed lines represent the results without a bare-baryon component. The experimental data are from Refs. [40–47].

that the $\Lambda(1405)$ contains little of the bare baryon component at infinite volume.

To explore the shape of the $\Lambda(1405)$, we show the $\pi\Sigma$ invariant mass distribution in Fig. 2. Here, the y axis represents $\omega_\pi^{\mathrm{cm}2}|T^0_{\pi\Sigma,\pi\Sigma}|^2 k_{\mathrm{cm}}^{\pi\Sigma}$ and the x axis indicates the $\pi\Sigma$ center-of-mass energy in units of MeV. The leading factor $\omega_\pi^{\mathrm{cm}2}$ is due to the convention of T. The solid (green) line is calculated from our scenario with the bare-baryon basis state. Results for the scenario without a bare baryon are very similar. The dashed (blue) histogram illustrates the experimental data from Ref. [49]. We note that the drop of the distribution from the peak is faster on the right in our case and is consistent with the experimental data.

B. Finite-volume results for varying quark masses

With the couplings determined and summarized in Table I, we can proceed to determine the finite-volume eigen-energy levels and associated components of the eigenstates by solving the eigenequation of the Hamiltonian $\mathcal{H}^0$ from Sec. II C. Of particular interest is the impact of the bare-baryon basis state in the finite volume of the lattice over a variety of pion masses.

TABLE I. Parameters constrained in our fits to cross sections of $K^- p$ and the pole positions obtained with these fit parameters in our two scenarios: one in which the $\Lambda(1405)$ is dynamically generated purely from the $\pi\Sigma$, $\bar K N$, $\eta\Lambda$, and $K\Xi$ interactions (No $|B_0\rangle$), and one also including a bare-baryon basis state to accommodate a three-quark configuration carrying the quantum numbers of the $\Lambda(1405)$ (with $|B_0\rangle$). The underlined entries indicate they are fixed in performing the fit.

Coupling	No $|B_0\rangle$	With $|B_0\rangle$
$g^0_{\pi\Sigma,\pi\Sigma}$	-1.77	-1.59
$g^0_{\bar K N,\bar K N}$	-2.14	-1.78
$g^0_{\bar K N,\pi\Sigma}$	0.78	0.89
$g^0_{\bar K N,\eta\Lambda}$	-0.42	-0.97
$g^0_{\pi\Sigma,K\Xi}$	-0.24	-0.56
$g^0_{\eta\Lambda,K\Xi}$	0.42	0.97
$g^0_{K\Xi,K\Xi}$	-0.60	-1.37
$g^0_{\pi\Sigma,B_0}$	$\cdots$	0.13
$g^0_{\bar K N,B_0}$	$\cdots$	0.16
$g^0_{\eta\Lambda}$	$\cdots$	-0.18
$g^0_{K\Xi}$	$\cdots$	-0.09
m_B^0/MeV	$\cdots$	1740
$g^1_{\pi\Sigma,\pi\Sigma}$	-0.14	$\underline{-0.14}$
$g^1_{\bar K N,\bar K N}$	-0.06	$\underline{-0.06}$
$g^1_{\bar K N,\pi\Sigma}$	1.36	$\underline{1.36}$
$g^1_{\bar K N,\pi\Lambda}$	0.96	$\underline{0.96}$
χ^2 (120 data)	166	177
Pole 1 (MeV)	$1428 - 23i$	$1429 - 22i$
Pole 2 (MeV)	$1333 - 85i$	$1338 - 89i$

To obtain results at larger pion masses, we need to know how the masses of the baryons and mesons vary with the quark mass ($\propto m_\pi^2$). For the bare mass, m_B^0, we use the linear assumption

$$m_B^0(m_\pi^2) = m_B^0|_{\mathrm{phys}} + \alpha_B^0(m_\pi^2 - m_\pi^2|_{\mathrm{phys}}), \qquad (18)$$

At larger quark masses, α_B^0 should be approximately $\frac{2}{3}\alpha_{N(1535)}^0 = 0.51\ \mathrm{GeV}^{-1}$ [34]. For each of the masses $m_N(m_\pi^2)$, $m_\Sigma(m_\pi^2)$, $m_K^2(m_\pi^2)$, etc., we use a linear interpolation between the corresponding lattice QCD results.

C. Conventional analysis

The results of the model in the absence of a bare-baryon basis state are illustrated in Fig. 3. Here we have used a linear interpolation between the CSSM results for the octet baryon masses. We observe that while the model can fit the lattice results at low pion masses, it fails at large pion

TABLE II. Pole positions for the $\Lambda(1405)$ in various approaches.

Approach	Pole 1 (MeV)	Pole 2 (MeV)
Refs. [20,48]	$1424^{+7}_{-23} - i26^{+3}_{-14}$	$1381^{+18}_{-6} - i81^{+19}_{-8}$
Ref. [6] fit I	$1417^{+4}_{-4} - i24^{+7}_{-4}$	$1436^{+14}_{-10} - i126^{+24}_{-28}$
Ref. [6] fit II	$1421^{+3}_{-2} - i19^{+8}_{-5}$	$1388^{+9}_{-9} - i114^{+24}_{-25}$
Ref. [21] solution 2	$1434^{+2}_{-2} - i10^{+2}_{-1}$	$1330^{+4}_{-5} - i56^{+17}_{-11}$
Ref. [21] solution 4	$1429^{+8}_{-7} - i12^{+2}_{-3}$	$1325^{+15}_{-15} - i90^{+12}_{-18}$
This work	$1430 - i22$	$1338 - i89$

masses. The results are very similar to those of Ref. [16], where the lattice results at large pion masses do not touch the curves given by the model.

The components of the eigenstates from the model without a bare-baryon basis state are presented in Fig. 4. Figures 4(a) and 4(b) reveal an avoided level crossing in the low-lying $\pi\Sigma$- and $\bar{K}N$-dominated states. At the lightest quark mass the first eigenstate is composed mainly of $\pi\Sigma$ while the second eigenstate is dominated by the $\bar{K}N$ component. The third state is composed of a nontrivial mix of the $\pi\Sigma$ and $\bar{K}N$ channels.

Only the second and third eigenstates are observed on the lattice. Consideration of the positions of the Hamiltonian model eigenstates relative to the dominant noninteracting basis states can provide some insight into the reasons for this. Both the $\pi\Sigma$- and $\bar{K}N$-dominated eigenstates sit below the noninteracting energies in Fig. 3, indicating significant attractive interactions. The small Compton wavelength of the kaon combined with attractive interactions with the

FIG. 3. The pion-mass dependence of the finite-volume energy eigenstates for the scenario without a bare-baryon basis state. The broken lines represent the noninteracting meson-baryon energies and the solid lines represent the spectrum derived from the matrix Hamiltonian model. The lattice QCD results are from the CSSM group [11,13], as described in Table III.

nucleon could provide significant clustering in the $\bar{K}N$ system. Such clustering increases the probability of finding the $\bar{K}$ next to the nucleon, thus increasing the overlap of the $\bar{K}N$-dominated state with the local three-quark operators used to excite the state [11]. Without this strong attraction the overlap is volume, V, suppressed with the probability of finding the meson next to the baryon $\propto 1/V$. In the case of the $\pi\Sigma$-dominated state the large Compton wavelength of the pion appears to reduce the level of clustering. We will return to this issue in the next section including a bare-baryon basis state.

Beyond the third quark mass considered, the lattice QCD results depart from the eigenstates of the Hamiltonian model. At these pion masses, the $\Lambda(1405)$ has become a stable state lying lower than the conventional $\pi\Sigma$ decay channel. As for the nucleon, one expects a dominant role for the simplest three-quark Fock-space component of the $\Lambda(1405)$ and the incorporation of a bare-basis state in the Hamiltonian model will be essential to describing
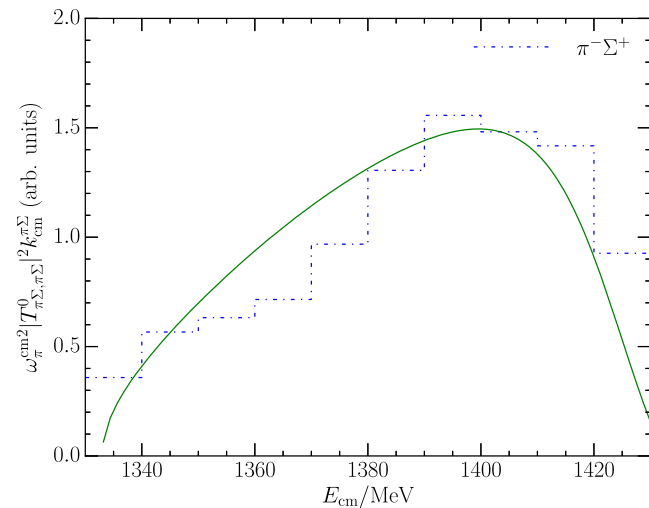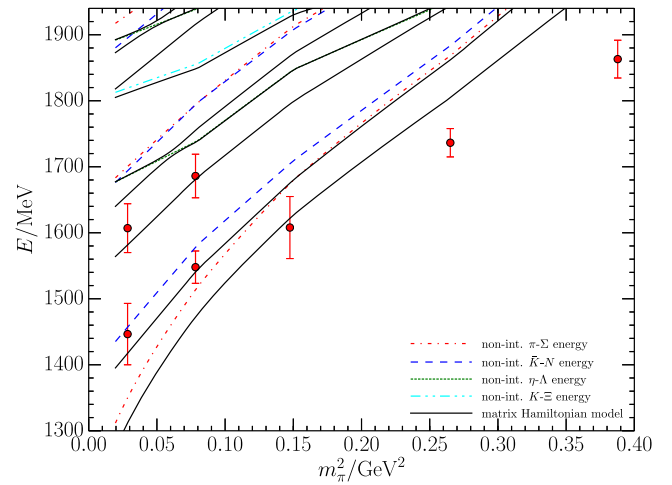
FIG. 2. The $\pi\Sigma$ invariant mass distribution. The solid (green) curve is calculated from the scenario with the bare-baryon basis state and the dashed (blue) histogram illustrates the experimental data from Ref. [49].

TABLE III. The low-lying odd-parity Λ masses provided by the CSSM group [11,13] with the strange-quark hopping parameter $\kappa_s = 0.13665$ tuned to reproduce the physical kaon mass [11]. Values for m_1 are from eigenstate-projected correlators dominated by the flavor-singlet interpolator [13] while values for m_2 are from projected correlators dominated by flavor-octet interpolators [11]. Values, provided with reference to the pion mass, are in units of GeV.

m_π	0.6233(7)	0.5148(7)	0.3890(10)	0.2834(6)	0.1742(26)
m_1	1.446(46)	1.548(24)	1.608(47)	1.736(21)	1.863(29)
m_2	$\cdots$	$\cdots$	$\cdots$	1.686(33)	1.607(37)

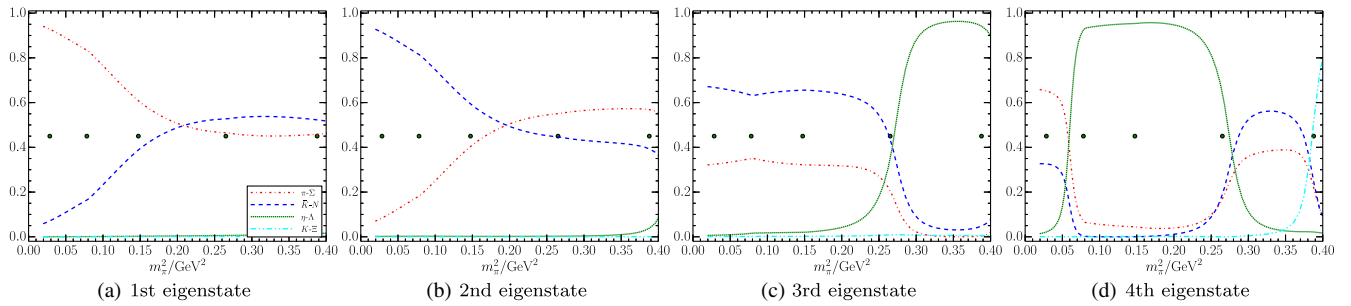|(a) 1st eigenstate | (b) 2nd eigenstate | (c) 3rd eigenstate | (d) 4th eigenstate |

FIG. 4.   The pion-mass evolution of the Hamiltonian eigenvector components for the first four states observed in the scenario without a bare-baryon basis state. Here all momenta for a particular meson-baryon channel have been summed to report the relative importance of the $\pi\Sigma$, $\bar{K}N$, $\eta\Lambda$, and $K\Xi$ channels. The (green) dots plotted horizontally at $y = 0.45$ indicate the positions of the five quark masses considered by the CSSM group on a lattice volume with $L \simeq 2.90$ fm.

these results. Drawing on the results of Ref. [50] for the ground-state nucleon, one can anticipate that the bare-baryon basis state will compose 80%–90% of the eigenvector components. Therefore, we do not trust the Hamiltonian model results of Fig. 4 at large quark masses.

D. Inclusion of a bare-baryon basis state

The inclusion of a bare-baryon basis state resolves the aforementioned discrepancies. The pion mass dependence of the odd-parity Λ spectrum incorporating the bare-baryon basis state is presented in Fig. 5. Figure 6 indicates the states receiving the largest contributions from the bare basis state.

Because local three-quark interpolating operators were used in exciting the states on the lattice, one would expect

that the states containing a significant bare-state component are easier to observe in lattice QCD. As a result, we label the low-lying states containing the largest bare-state components by superposing thick (colored) lines on them in Fig. 5. In a successful description, the lattice results would correspond to these labeled states.

For example, the integers next to the solid red curve in Fig. 6 indicate that the most probable state to be observed in lattice QCD simulations with local three-quark operators is the fourth eigenstate at the lightest quark mass considered, becoming the third eigenstate for the second and third quark masses with $0.06 \leq m_\pi^2 \leq 0.16$ GeV^2. As m_π^2 continues to increase, the most probable state falls to the second eigenstate briefly, before settling on the lowest-lying state at the largest quark masses considered.
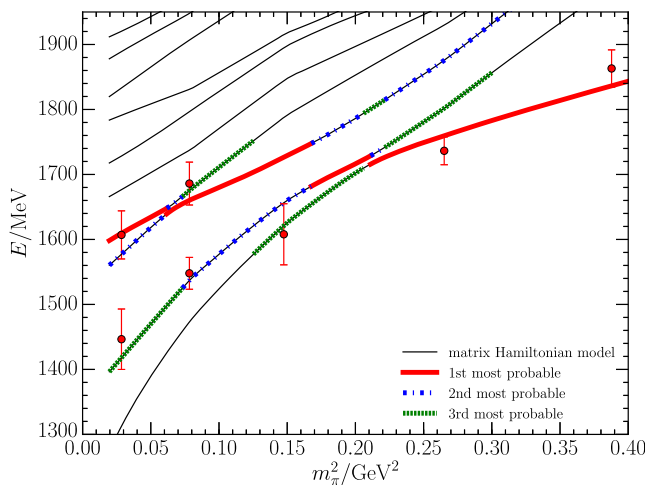

FIG. 5.   The pion-mass dependence of the finite-volume energy eigenstates for the scenario including a bare-baryon basis state. The different line types and colors used in illustrating the energy levels indicate the strength of the bare basis state in the Hamiltonian-model eigenvector. The thick-solid (red), dashed (blue) and short-dashed (green) lines correspond to the first, second, and third strongest bare-state contributions, and therefore the most likely states to be observed with three-quark interpolating fields.
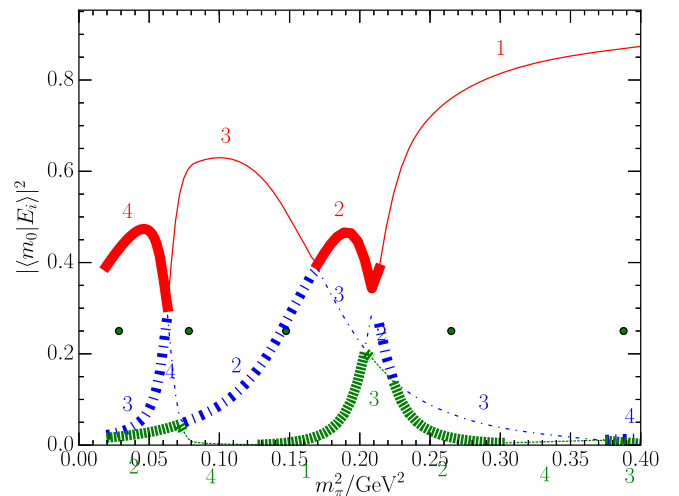

FIG. 6.   The fraction of the bare-baryon basis state, $|m_0\rangle$, in the Hamiltonian energy eigenstates $|E_i\rangle$ for the three low-lying states having the largest bare-state contribution. States are labeled by the energy-eigenstate integers i indicated next to the curves. The dark-green dots plotted at $y = 0.25$ indicate the positions of the five quark masses considered in the CSSM results. While the line type and color scheme matches that of Fig. 5, the thick and thin lines alternate to indicate a change in the energy eigenstate.

Consideration of the three most probable states to be seen in the lattice QCD calculations is sufficient to explain the states observed in the lattice QCD calculations. At each mass, the lowest-lying probable state(s) are observed. The second excitations [11] observed on the lattice at the lightest two quark masses considered also agree with the energies of the most probable states to be seen.

In contrast, the lowest-lying $\pi\Sigma$-dominated state at light quark masses has a negligible bare-state component and therefore is not observed in the lattice QCD spectrum obtained with local three-quark operators. Instead, the lowest-lying lattice results correspond to the second eigenstate which has both a bare-state contribution and the benefit of clustering in the $\bar{K}N$ channel as discussed in Sec. III C. Figure 7 illustrates the positions of the Hamiltonian model eigenstate energies relative to the noninteracting meson-baryon basis-state energies, indicating attractive interactions. Five-quark lattice operators with the momentum of both the π and Σ hadrons projected to zero are expected to reveal the lowest-lying $\pi\Sigma$-dominated state predicted by the Hamiltonian model.

The basis state components of the eigenstates for this scenario incorporating a bare-baryon basis state are illustrated in Fig. 8. Considering Fig. 8(a), one observes that the first eigenstate is $\pi\Sigma$ dominated at small pion masses. It transitions briefly to a significant $\bar{K}N$ component and is eventually dominated by the bare-baryon basis state at large pion masses. Comparing Figs. 3 and 5, it is apparent that the bare baryon is vital to describing the lattice QCD results for the $\Lambda(1405)$.

The uncertainty on the lattice QCD result at the middle quark mass considered ($m_\pi^2 = 0.15$ GeV^2) is unusually large due to difficulty in identifying a plateau in the

effective mass with an acceptable $\chi^2_{\rm dof}$ at early Euclidean times. Extensive Euclidean time evolution isolated the lowest state in the spectrum at the expense of a larger uncertainty. The origin of the difficulty is now clear. There are two nearby states in the spectrum at this quark mass, both having significant overlap with the three-quark interpolating fields used. Both the first and second Hamiltonian eigenstates have large attractive $\bar{K}N$ components and both states have nontrivial bare state components. While the second state has a larger bare state component, Euclidean time evolution will eventually favor the lower-lying state. At moderate Euclidean times, a superposition of states is encountered, accompanied by a large $\chi^2_{\rm dof}$ in the single-state ansatz. Further Euclidean time evolution favors the lower-lying state and the single-state $\chi^2_{\rm dof}$ becomes acceptable.

At lighter quark masses, the first Hamiltonian eigenstate has a negligible bare-state component. The second Hamiltonian eigenstate has both the attractive $\bar{K}N$ component and a nontrivial bare-state component and is therefore seen on the lattice. The fourth and third Hamiltonian model eigenstates capture the largest bare-state components at the lightest and second-lightest quark masses considered respectively and are associated with the lattice QCD eigenstates dominated by SU(3)-flavor-octet interpolating fields.

It is interesting to compare the spectra and structure observed herein at light quark masses with the analysis of Ref. [16]. Comparing Fig. 7 here with Fig. 1 of Ref. [16] for the spectrum, both spectra commence with a bound state below the $\pi\Sigma$ threshold at small pion masses. Consistently, the lowest lattice QCD results correspond to the second eigenstate for small m_π. The third eigenstate energies are both above 1500 MeV. However, the third eigenstate energy reported herein is 50 MeV larger at the physical pion mass. At this energy, there is a desire to consider experimental data at higher energies to better constrain the models and improve the accuracy of the predictions. In both works, four eigenstates are predicted below 1.6 MeV.

With regard to the composition of the states, we can compare Table III of Ref. [16] with Fig. 8 in our work. At the physical pion mass, both analyses indicate the first and fourth eigenstates are dominated by $\pi\Sigma$ basis states while the second and third eigenstates are dominated by $\bar{K}N$ basis states.

Turning our attention to the quark-mass dependence of the spectrum, the isospin-zero bare-mass state is associated with the lowest-lying state observed in lattice QCD calculations at large quark masses. However, as one moves away from the flavor-symmetric limit towards the light quark-mass regime and flavor symmetry is broken, this bare mass becomes associated with the low-lying flavor-octet dominated states. As m_π^2 decreases, the first shift of the bare mass from state 1 to state 2 occurs at the avoided level crossing of the $\pi\Sigma$ and $\Lambda(1405)$ at $m_\pi^2 = 0.21$ GeV^2, easily identified in Fig. 5. Shortly thereafter, Hamiltonian-model eigenstate 1 becomes $\pi\Sigma$ dominated and the
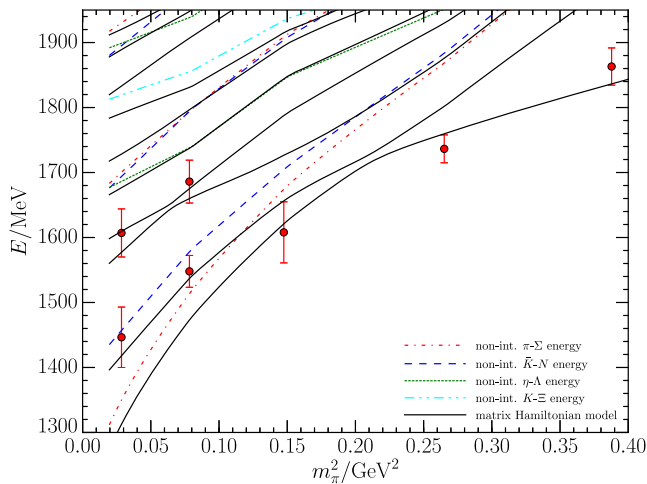

FIG. 7. The pion-mass dependence of the finite-volume energy eigenstates for the scenario including a bare-baryon basis state. The broken lines represent the noninteracting meson-baryon energies and the solid lines represent the spectrum derived from the matrix Hamiltonian model.

(a) 1st eigenstate   (b) 2nd eigenstate   (c) 3rd eigenstate   (d) 4th eigenstate
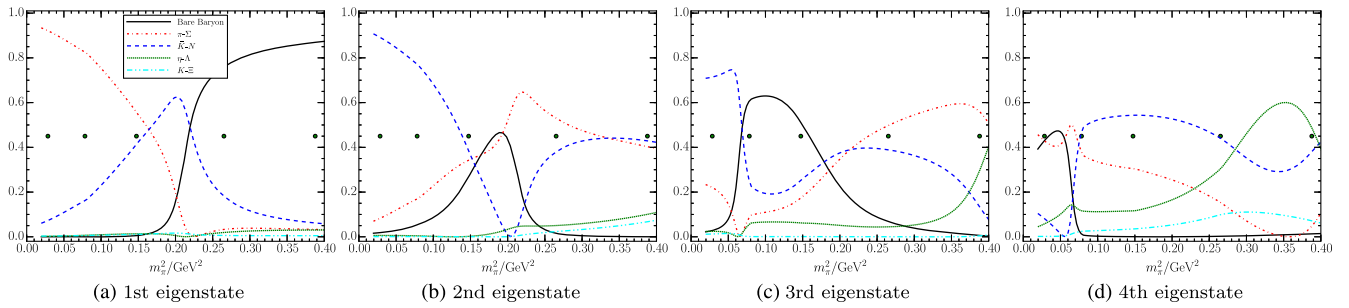
FIG. 8. The pion-mass evolution of the Hamiltonian eigenvector components for the first four states observed in the scenario incorporating a bare-baryon basis state contribution. Again, all momenta for a particular meson-baryon channel have been summed to report the relative importance of the meson-baryon channels. The (green) dots plotted horizontally at $y = 0.45$ indicate the positions of the five quark masses considered by the CSSM group on a lattice volume with $L \simeq 2.90$ fm.

Λ(1405) moves to the second eigenstate. Moving to lighter quark masses, the bare mass shifts to the flavor-octet dominated states while the flavor-singlet dominated Λ(1405) evolves to become predominantly $\bar{K}N$, in accord with the conclusions of Ref. [13]. Its energy is around 1.446(46) GeV near the physical pion mass. From Fig. 8(b), it is composed of about 90% $\bar{K}N$, a few percent $\pi\Sigma$, and a small amount of the bare-baryon basis state.

IV. SUMMARY

We have studied the cross sections for K^-p scattering at low energies using effective field theory. We considered two scenarios in constructing the basis states of our models: one in which the Λ(1405) is dynamically generated purely from the $\pi\Sigma$, $\bar{K}N$, $\eta\Lambda$, and $K\Xi$ interactions, and one also including a bare baryon to accommodate a three-quark configuration carrying the quantum numbers of the Λ(1405). Both scenarios produce two poles in the regime of the Λ(1405) resonance, with values in accord with other studies.

With the parameters of the model constrained by the experimental data, Hamiltonian effective field theory was used to calculate the finite-volume spectrum of states in our two scenarios and confront lattice QCD data for the low-lying odd-parity Λ spectrum in a finite volume with length $L \sim 2.9$ fm.

At large quark masses, the bare state is vital to obtaining an accurate description of the Λ(1405). Here the state is stable with a structure dominated by an 80%–90% bare-state component, similar to that for the ground-state nucleon. At smaller quark masses, the presence of the bare-baryon basis state in the Hamiltonian model eigenvector explains which states are seen in current lattice QCD calculations and which states are missed with local three-quark operators on the lattice.

It is apparent that the nature of the Λ(1405) changes dramatically as the light quark mass is varied. At large quark masses, the bare-baryon state is associated with the lowest-lying state observed in lattice QCD calculations. This state is excited by an interpolating field dominated by SU(3)-flavor-singlet operators. As one moves towards the light quark-mass regime, the bare basis state becomes affiliated with the lattice QCD eigenstates excited by interpolating fields dominated by flavor-octet operators. After an avoided level crossing with the $\pi\Sigma$-dominated state, the Λ(1405) becomes the second state in the spectrum and evolves to become a state dominated by $\bar{K}N$ components. These results are consistent with the earlier findings of Ref. [13] based on the strange quark contribution to the magnetic form factor of the Λ(1405).

Neither the cross sections for K^-p scattering nor the pole positions in the S-matrix are sensitive to the bare-baryon basis state and this indicates that the physical resonance also has only a small bare-state component in its composition. Together, these findings confirm that the Λ(1405) is predominantly a molecular $\bar{K}N$ bound state.

[1] N. Kaiser, T. Waas, and W. Weise, Nucl. Phys. **A612**, 297 (1997).

[2] E. Oset and A. Ramos, Nucl. Phys. **A635**, 99 (1998).

[3] J. Oller and U.-G. Meißner, Phys. Lett. B **500**, 263 (2001).

[4] T. Hyodo, S.-i. Nam, D. Jido, and A. Hosaka, Prog. Theor. Phys. **112**, 73 (2004).

[5] Y. Ikeda, T. Hyodo, and W. Weise, Phys. Lett. B **706**, 63 (2011).

[6] Z.-H. Guo and J. A. Oller, Phys. Rev. C **87**, 035202 (2013).

[7] M. Mai and U.-G. Meißner, Nucl. Phys. **A900**, 51 (2013).

[8] Y. Akaishi, K. S. Myint, and T. Yamazaki, Proc. Jpn. Acad., Ser. B **84**, 264 (2008).

[9] A. W. Thomas, S. Theberge, and G. A. Miller, Phys. Rev. D **24**, 216 (1981).

[10] A. W. Thomas, Adv. Nucl. Phys. **13**, 1 (1984).

[11] B. J. Menadue, W. Kamleh, D. B. Leinweber, and M. S. Mahbub, Phys. Rev. Lett. **108**, 112001 (2012).

[12] G. P. Engel, C. B. Lang, and A. Schäfer (BGR [Bern-Graz-Regensburg] Collaboration), Phys. Rev. D **87**, 034502 (2013).

[13] J. M. M. Hall, W. Kamleh, D. B. Leinweber, B. J. Menadue, B. J. Owen, A. W. Thomas, and R. D. Young, Phys. Rev. Lett. **114**, 132002 (2015).

[14] J. M. M. Hall et al., Proc. Sci., LATTICE2014 (2014) 094.

[15] R. D. Young, D. B. Leinweber, A. W. Thomas, and S. V. Wright, Phys. Rev. D **66**, 094507 (2002).

[16] R. Molina and M. Doring, Phys. Rev. D **94**, 056010 (2016).

[17] G. Rajasekaran, Phys. Rev. D **5**, 610 (1972).

[18] D. B. Leinweber, Ann. Phys. (N.Y.) **198**, 203 (1990).

[19] T. Hyodo, D. Jido, and A. Hosaka, Phys. Rev. C **78**, 025203 (2008).

[20] Y. Ikeda, T. Hyodo, and W. Weise, Nucl. Phys. **A881**, 98 (2012).

[21] M. Mai and U.-G. Meißner, Eur. Phys. J. A **51**, 30 (2015).

[22] A. Cieplý, M. Mai, U.-G. Meißner, and J. Smejkal, Nucl. Phys. **A954**, 17 (2016).

[23] C. Fernández-Ramírez, I. V. Danilkin, D. M. Manley, V. Mathieu, and A. P. Szczepaniak (Joint Physics Analysis Center), Phys. Rev. D **93**, 034029 (2016).

[24] Y. Kamiya, K. Miyahara, S. Ohnishi, Y. Ikeda, T. Hyodo, E. Oset, and W. Weise, Nucl. Phys. **A954**, 41 (2016).

[25] S. Ohnishi, Y. Ikeda, T. Hyodo, and W. Weise, Phys. Rev. C **93**, 025207 (2016).

[26] D. Jido, J. A. Oller, E. Oset, A. Ramos, and U.-G. Meißner, Nucl. Phys. **A725**, 181 (2003).

[27] E. A. Veit, B. K. Jennings, R. C. Barrett, and A. W. Thomas, Phys. Lett. **137B**, 415 (1984).

[28] E. A. Veit, B. K. Jennings, A. W. Thomas, and R. C. Barrett, Phys. Rev. D **31**, 1033 (1985).

[29] A. Cieply and J. Smejkal, Nucl. Phys. **A881**, 115 (2012).

[30] A. Mueller-Groeling, K. Holinde, and J. Speth, Nucl. Phys. **A513**, 557 (1990).

[31] J. Haidenbauer, G. Krein, U.-G. Meissner, and L. Tolos, Eur. Phys. J. A **47**, 18 (2011).

[32] M. Doring, J. Haidenbauer, U.-G. Meissner, and A. Rusetsky, Eur. Phys. J. A **47**, 163 (2011).

[33] J. M. M. Hall, A. C.-P. Hsu, D. B. Leinweber, A. W. Thomas, and R. D. Young, Phys. Rev. D **87**, 094510 (2013).

[34] Z.-W. Liu, W. Kamleh, D. B. Leinweber, F. M. Stokes, A. W. Thomas, and J.-J. Wu, Phys. Rev. Lett. **116**, 082004 (2016).

[35] J.-J. Wu, T.-S. H. Lee, A. W. Thomas, and R. D. Young, Phys. Rev. C **90**, 055206 (2014).

[36] D. Leinweber et al., JPS Conf. Proc. **10**, 010011 (2016).

[37] R. D. Young, D. B. Leinweber, and A. W. Thomas, Prog. Part. Nucl. Phys. **50**, 399 (2003).

[38] J. M. M. Hall, D. B. Leinweber, and R. D. Young, Phys. Rev. D **82**, 034010 (2010).

[39] E. A. Veit, A. W. Thomas, and B. K. Jennings, Phys. Rev. D **31**, 2242 (1985).

[40] G. S. Abrams and B. Sechi-Zorn, Phys. Rev. **139**, B454 (1965).

[41] M. Sakitt, T. B. Day, R. G. Glasser, N. Seeman, J. Friedman, W. E. Humphrey, and R. R. Ross, Phys. Rev. **139**, B719 (1965).

[42] J. K. Kim, Phys. Rev. Lett. **14**, 29 (1965).

[43] M. Csejthey-Barth et al., Phys. Lett. **16**, 89 (1965).

[44] T. S. Mast, M. Alston-Garnjost, R. O. Bangerter, A. S. Barbaro-Galtieri, F. T. Solmitz, and R. D. Tripp, Phys. Rev. D **14**, 13 (1976).

[45] R. O. Bangerter, M. Alston-Garnjost, A. Barbaro-Galtieri, T. S. Mast, F. T. Solmitz, and R. D. Tripp, Phys. Rev. D **23**, 1484 (1981).

[46] J. Ciborowski et al., J. Phys. G **8**, 13 (1982).

[47] D. Evans, J. V. Major, E. Rondio, J. A. Zakrzewski, J. E. Conboy, D. J. Miller, and T. Tymieniecka, J. Phys. G **9**, 885 (1983).

[48] M. P. Valderrama, Phys. Rev. D **85**, 114037 (2012).

[49] R. J. Hemingway, Nucl. Phys. **B253**, 742 (1985).

[50] Z.-W. Liu et al., arXiv:1607.04536.